Generation of the ^{1}H in H_2O neutron thermal scattering law covariance matrix of the CAB model

Juan Pablo Scotta, Gilles Noguère, Jose Ignacio Marquez Damian

▶ **To cite this version:**

Juan Pablo Scotta, Gilles Noguère, Jose Ignacio Marquez Damian. Generation of the ^{1}H in H_2O neutron thermal scattering law covariance matrix of the CAB model. EPJ N - Nuclear Sciences & Technologies, 2018, 4, pp.32. 10.1051/epjn/2018024 . cea-02305793

HAL Id: cea-02305793

https://cea.hal.science/cea-02305793v1

Submitted on 4 Oct 2019

HAL is a multi-disciplinary open access archive for the deposit and dissemination of scientific research documents, whether they are published or not. The documents may come from teaching and research institutions in France or abroad, or from public or private research centers.

L'archive ouverte pluridisciplinaire **HAL**, est destinée au dépôt et à la diffusion de documents scientifiques de niveau recherche, publiés ou non, émanant des établissements d'enseignement et de recherche français ou étrangers, des laboratoires publics ou privés.

Distributed under a Creative Commons Attribution 4.0 International License

EPJ Nuclear Sci. Technol. 4, 32 (2018)
© J.P. Scotta et al., published by EDP Sciences, 2018
https://doi.org/10.1051/epjn/2018024

EPJ Nuclear Sciences & Technologies

Available online at:
https://www.epj-n.org

Regular Article

Open Access

Generation of the ^{1}H in H_2O neutron thermal scattering law covariance matrix of the CAB model

Juan Pablo Scotta[1], Gilles Noguère[1,*], and Jose Ignacio Marquez Damian[2]

[1] CEA, DEN, DER Cadarache, Saint Paul les Durance, France
[2] Neutron Physics Departement and Instituto Balseiro, Centro Atomico Bariloche, CNEA, San Carlos de Bariloche, Argentina

Received: 12 October 2017 / Received in final form: 13 February 2018 / Accepted: 14 May 2018

Abstract. The thermal scattering law (TSL) of ^{1}H in H_2O describes the interaction of the neutron with the hydrogen bound to light water. No recommended procedure exists for computing covariances of TSLs available in the international evaluated nuclear data libraries. This work presents an analytic methodology to produce such a covariance matrix-associated to the water model developed at the Atomic Center of Bariloche (Centro Atomico Bariloche, CAB, Argentina). This model is called as CAB model, it calculates the TSL of hydrogen bound to light water from molecular dynamic simulations. The performance of the obtained covariance matrix has been quantified on integral calculations at "cold" reactor conditions between 20 and 80 °C. For UOX fuel, the uncertainty on the calculated reactivity ranges from ±71 to ±155 pcm. For MOX fuel, it ranges from ±110 to ±203 pcm.

1 Introduction

The calculation of a critical system is carried out by means of reactor physics simulation code that uses evaluated nuclear data. The evaluated nuclear data libraries contain reaction information necessary to quantify the neutronic parameters that describe the behavior of the system. In light water reactor calculations, neutrons are slowed down by the ^{1}H in H_2O inelastic thermal scattering data, which are expressed in terms of thermal scattering law (TSL). The TSL describes the dynamics of the scattering target and gives information about the energy and angle of the scattered neutrons. To evaluate the safety margins, the uncertainties coming from the nuclear data have to be assessed. However, no covariance information for the TSL of ^{1}H in H_2O is available in any nuclear data library.

Mathematical frameworks for producing covariance matrix for the TSL exist. In a previous work, a Monte-Carlo methodology was developed and applied to hexagonal graphite [1]. A different procedure based on an analytic method was also recently proposed [2]. It was applied to the TSL of ^{1}H in H_2O-associated to the JEFF-3.1.1 nuclear data library [3].

A new model for light water, namely the CAB model, was developed at the atomic center of Bariloche in Argentina [4]. The originality of this model relies on the use of molecular dynamic simulations for calculating the density of states of hydrogen in the water molecule. The objective of the present work is to produce a covariance matrix between the CAB model parameters and to test its performance on integral calculations between 20 and 80 °C.

2 Thermal inelastic neutron scattering

A description of the thermal scattering theory can be found in references [5,6]. In this section, an introductory background will be given to set the basis for the present work.

Working in the incoherent approximation, the total cross section of H_2O as a function of the incident neutron energy E_n is given by:

$$\sigma_T^{H_2O}(E_n) = 2\sigma_T^H(E_n) + \sigma_T^O(E_n), \quad (1)$$

where σ_T^O is the total cross section of ^{16}O and σ_T^H is the total cross section of ^{1}H which is given by:

$$\sigma_T^H(E_n) = \sigma_\gamma(E_n) + \sigma_n(E_n). \quad (2)$$

For light isotopes, in the thermal energy range, the capture cross section $\sigma_\gamma(E_n)$ can be approximated as:

$$\sigma_\gamma(E_n) = \sigma_{\gamma 0}\sqrt{\frac{E_0}{E_n}}, \quad (3)$$

where $\sigma_{\gamma 0}$ is the capture cross section measured at the thermal neutron energy ($E_0 = 25.3$ meV).

* e-mail: gilles.noguere@cea.fr

This is an Open Access article distributed under the terms of the Creative Commons Attribution License (http://creativecommons.org/licenses/by/4.0), which permits unrestricted use, distribution, and reproduction in any medium, provided the original work is properly cited.

In the low energy range, typically below 5 eV, the slowing down of neutrons in water is affected by the chemical bonds between the hydrogen and oxygen atoms. Such impact is taken into account in the neutronic calculations by using the double differential scattering cross section:

$$\sigma_n(E_n) = \int\int \frac{d^2\sigma_n}{d\theta\, dE} d\theta\, dE. \tag{4}$$

The double differential cross section expresses the probability that an incident neutron of energy E_n will be scattered at a secondary energy E and direction θ. If T is the temperature of the target and k_B is the Boltzmann constant, the double differential scattering cross section for ^{1}H in H_2O is calculated as [7]:

$$\frac{d^2\sigma_n}{d\theta\, dE} = \frac{\sigma_b}{4\pi k_B T}\sqrt{\frac{E}{E_n}} e^{\frac{-\beta}{2}} S(\alpha\beta), \tag{5}$$

where σ_b is the bound scattering cross section of hydrogen and $S(\alpha, \beta)$ is the so-called thermal self-scattering function (or alternatively thermal scattering law), defined as a function of the dimensionless momentum transfer α and energy transfer β:

$$\alpha = \frac{E + E_n - 2\sqrt{EE_n}\mu}{Ak_BT}, \tag{6}$$

$$\beta = \frac{E - E_n}{k_BT}, \tag{7}$$

where μ is the cosine of the scattering angle θ ($\mu = \cos(\theta)$) in the laboratory system and A is the ratio of the scattering target to the neutron mass.

In practice, the calculation of the scattering law is performed with the LEAPR module of the NJOY processing system [8], in which the key parameter is the frequency spectrum $\rho(\beta)$ of ^{1}H in H_2O. The frequency spectrum characterizes the excitations states of the material. In the CAB model, it is introduced in the LEAPR module as a decomposition of three partial spectra:

$$\rho(\beta) = \sum_{i=1}^{2} \omega_i \delta(\beta_i) + \omega_t \rho_t(\beta) + \omega_c \rho_c(\beta). \tag{8}$$

The discrete oscillators are represented by $\delta(\beta_i)$ for $i = 1, 2$. They describe the intramolecular modes of vibration, where β_i is the energy and ω_i the associated weight. The continuous frequency distribution $\rho_c(\beta)$ models the intermolecular modes. The weight corresponding to this partial spectrum is ω_c. Finally, ρ_t accounts for the translation of the molecule.

3 The CAB model

The frequency spectrum of ^{1}H in H_2O of the CAB model [4] was calculated using the molecular dynamic simulation code GROMACS [9]. The water potential implemented in the code was the TIP4P/2005f potential [10].

Table 1. Parameters of the TIP4P/2005f water potential [10] as used in the CAB model established in reference [4].

Parameter	Value
σ_0 (nm)	3.1644
ε_0 (kJ/mol)	0.7749
q_H (e^-)	0.5564
q_M (e^-)	−1.1128
d_{OH} (nm)	0.09419
D_{OH} (kJ/mol)	432.581
β_{OH} (1/nm)	22.87
θ_{OH} (°)	107.4
k_θ (kJ/mol/rad^2)	367.81
d_{OM} (nm)	0.15555

3.1 The parameters of the CAB model

The parameters of the CAB model correspond to the TIP4P/2005f water potential. This potential is a flexible potential with four positions: two hydrogen atoms, one oxygen and one so-called M-site (dummy atom). The dummy atom is located over the angle bisector formed by the two hydrogens and the oxygen. Table 1 lists the TIP4P/2005f water potential parameters used in the CAB model.

The intermolecular interactions are represented by a Lennard-Jones potential V_{LJ} between the oxygen atoms:

$$V_{LJ}(r_{ij}) = 4\varepsilon_0\left[\left(\frac{\sigma_0}{r_i - r_j}\right)^{12} - \left(\frac{\sigma_0}{r_i - r_j}\right)^{6}\right], \tag{9}$$

and the Coulomb potential V_c is given by:

$$V_c(r_{ij}) = k\frac{q_i q_j}{r_{ij}}, \tag{10}$$

where ε_0 is the depth of the potential well, σ_0 represents the distance where the potential is zero, k is the Coulomb constant, q_i is the electrical charge of the particle and r_{ij} stands for the distance between two atoms.

The intramolecular interactions are characterized by a Morse potential V_M. It accounts the stretching of the hydrogen–oxygen bond as follows:

$$V_M(r_{ij}) = D_{OH}\left[1 - e^{-\beta_{OH}(r_{ij} - d_{OH})}\right]. \tag{11}$$

For the bending mode, the harmonic angle potential V_{HOH} is:

$$V_{HOH}(\theta_{ij}) = \frac{1}{2}k_\theta(\theta_{ij} - \theta_0)^2. \tag{12}$$

In the above equations, D_{OH} is the depth of the potential well, β_{OH} is the steepness of the well, d_{OH} is the equilibrium distance between the oxygen and the hydrogen, k_θ the strength constant and θ_0 is the equilibrium angle between the hydrogens and oxygen.

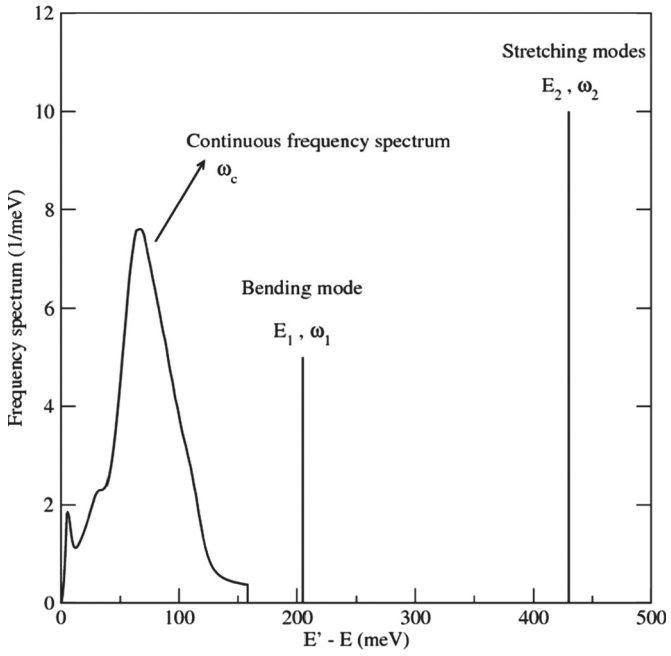

Fig. 1. Continuous frequency spectrum of ^{1}H in H_2O and internal vibration modes ($E_1 = 205$ meV and $E_2 = 415$ meV) of the CAB model as a function of the excitation energy at $T = 294$ K.

3.2 Frequency spectrum of ^{1}H in H_2O used in the CAB model

In the CAB model, the translational mode is modeled with the Egelstaff-Schofield diffusion model [11]. The continuous frequency spectrum of ^{1}H in H_2O is then obtained by subtracting the Egelstaff-Schofield spectrum to the generalized frequency spectrum obtained from molecular dynamic simulations [4].

The continuous frequency spectrum of ^{1}H in H_2O as well as the discrete oscillators modeling the intramolecular modes at 294 K are shown in Figure 1. The continuous spectrum is dominated by the libration mode ($\simeq$70 meV). The structures of small amplitude observed at very low energy transfer ($\simeq$5 and $\simeq$30 meV) were observed experimentally [12] and are still visible even with a rigid model [13]. They should correspond to vibrational modes between the hydrogen and oxygen atoms of different water molecules.

The translational weight ω_t, involved in the Egelstaff-Schofield diffusion model, was deduced from experimental measures of Novikov [14] of diffusion masses for light water at different temperatures. Table 2 summarizes the LEAPR parameters of the CAB model at 294 K and the weights corresponding to each vibration mode.

3.3 The average cosine of the scattering angle calculated with the CAB model in the laboratory system

The integration over the secondary energy E of equation (5) gives the simple differential cross section (or angular distribution). The average for each incident neutron energy

Table 2. CAB model parameters introduced in the LEAPR module [8] for ^{1}H in HO at 294 K [4].

Parameter	Value
Translational weight ω_t	7.918^{-3}
Continuous spectrum weight ω_c	0.522
Bending mode energy E_1 (meV)	205.0
Bending mode weight ω_1	0.157
Stretching modes energy E_2 (meV)	415.0
Stretching mode weight ω_2	0.313
Diffusion constant c	3.969
Free scattering cross section σ_b^H (b)	20.478

gives the average cosine $\overline{\mu}$ of the scattering angle:

$$\overline{\mu}(E_n) = \frac{\int_0^\pi \cos\theta \sin\theta \left(\int_0^\infty \frac{d^2\sigma_n}{d\theta\, dE} dE \right) d\theta}{\int_0^\pi \sin\theta \left(\int_0^\infty \frac{d^2\sigma_n}{d\theta\, dE} dE \right) d\theta}. \quad (13)$$

In Figure 2 it is compared the data measured by Beyster et al. [15] and the average cosine of the scattering angle calculated with the CAB model at 294 K. An overall good agreement is obtained between the calculated curve and the data.

3.4 The H_2O total cross section calculated with the CAB model

The total cross section $\sigma_T^{H_2O}$ calculated with the CAB model at 294 K is shown in Figure 3. The theoretical curve is compared with a set of selected data measured at room temperature [16–19]. The CAB model correctly reproduces the measured values over the full energy range. Therefore, the generation of the covariance matrix will consists of determining the uncertainties of the CAB model parameters without changing their values.

4 Methodology for producing covariance matrices with the CONRAD code

The covariance matrix between the CAB model parameters was analytically calculated using the CONRAD (code for nuclear reaction analysis and data assimilation) code [20]. The methodology relies on a generalized least-square fitting algorithm and on the marginalization technique.

4.1 The generalized least-square method

The generalized least-square method implemented in the CONRAD code is designed to provide a set of best-estimate model parameters given a set of experimental data. It is based on the Bayes theorem [21], which states that the posterior information of a quantity is proportional to the prior, times a likelihood function, which yields the probability to obtain an experimental data set $\vec{y}$ for a given model parameters $\vec{x}$.

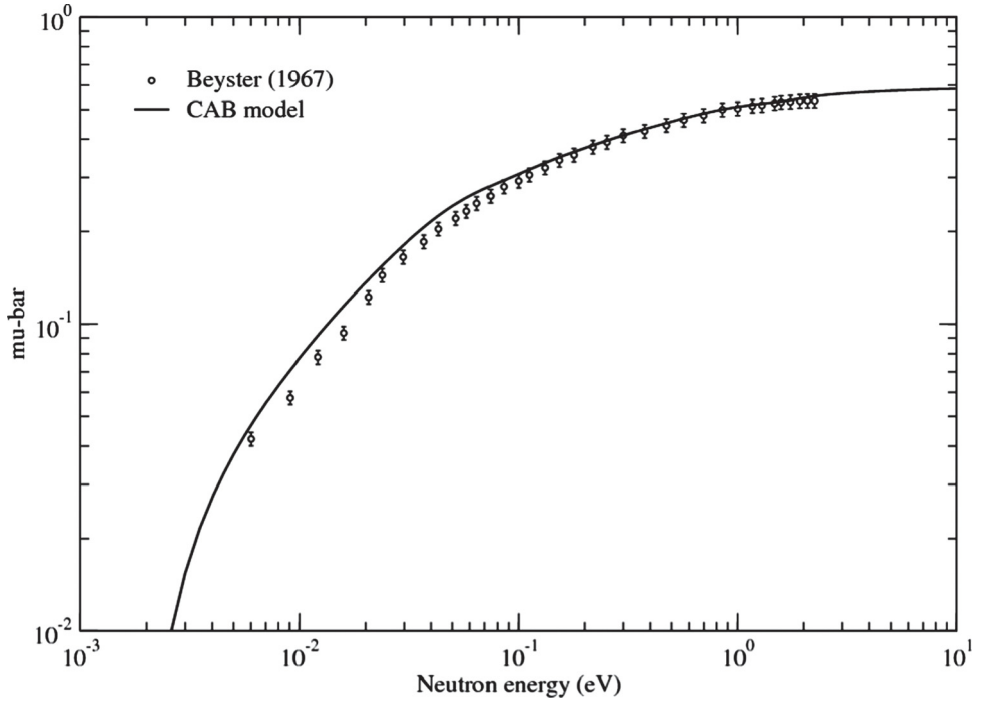

Fig. 2. Average cosine of the scattering angle calculated with the CAB model compared with experimental data at 294 K [15].

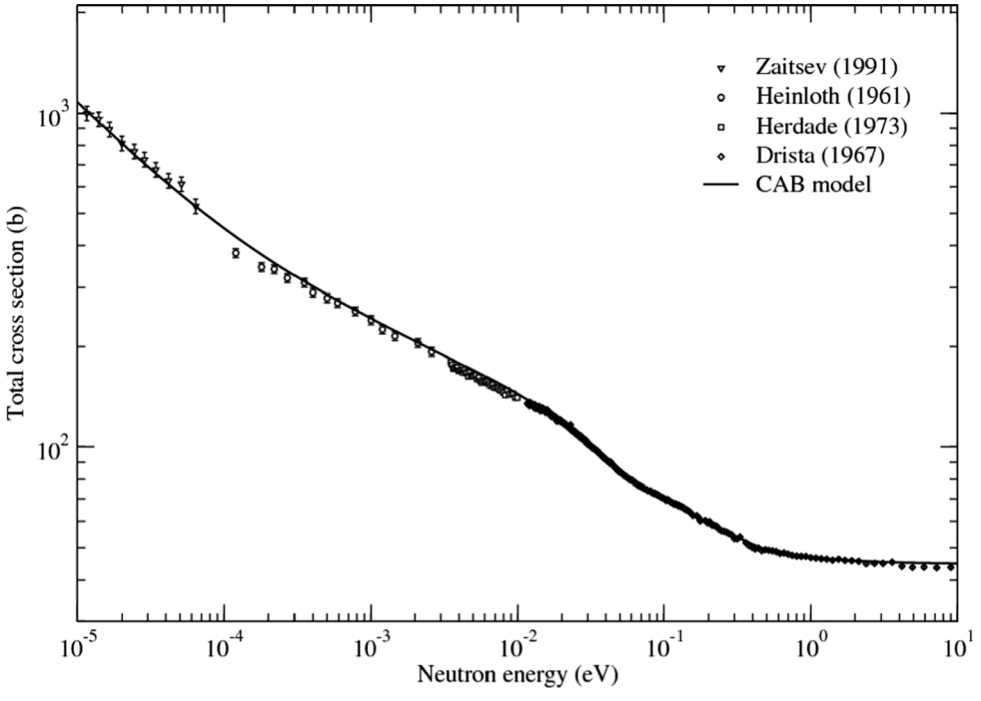

Fig. 3. Total cross section calculated with the CAB model at 294 K compared with experimental data [16–19].

In the CONRAD code, the procedure consists of resolving iteratively by the Newton–Raphson method the following sets of equations for the model parameter $\vec{x}$ and covariance matrix M_x [22]:

$$\vec{x}^{\,i} = \vec{x}^{\,i-1} M_x^i \left(G_x^{i-1}\right)^T \left(M_y\right)^{-1} \left(\vec{y} - \vec{t}^{\,i-1}\right), \qquad (14)$$

$$\left(M_x^i\right)^{-1} = \left(M_x^{i-1}\right)^{-1} \left(G_x^{i-1}\right)^T \left(M_y\right)^{-1} G_x^{i-1}, \qquad (15)$$

where M_y is the experimental covariance matrix and $\vec{t}$ is the theoretical model. The matrix G_x is the derivative matrix of the theoretical model with respect to the parameters $\vec{x}$:

$$G_x = \begin{pmatrix} \frac{\partial t_1}{\partial x_1} & \cdots & \frac{\partial t_1}{\partial x_n} \\ \vdots & & \vdots \\ \frac{\partial t_k}{\partial x_n} & \cdots & \frac{\partial t_k}{\partial x_1} \end{pmatrix}. \quad (16)$$

4.2 The marginalization technique

The marginalization technique was designed to take into account the uncertainties of systematic origin in the nuclear data evaluating process. Such type of uncertainties usually introduce strong correlations between the experimental values.

These parameters, called nuisance parameters, correspond to the aspect of physical realities whose properties are not of particular interest as such but are fundamental for assessing reliable model parameters [23].

If $\vec{\theta} = (\theta_1, \ldots, \theta_m)$ is the nuisance parameter vector and M_θ stands for the covariance matrix, then the posterior covariance matrix after the marginalization M_x^{marg} is obtained as [24]:

$$M_x^{marg} = M_x + \left(G_x^T G_x\right)^{-1} G_x^T G_\theta M_\theta G_\theta^T G_x \left(G_x^T G_x\right)^{-1}, \quad (17)$$

where the matrix G_θ is the derivative matrix of the theoretical model with respect to the nuisance parameters vector:

$$G_\theta = \begin{pmatrix} \frac{\partial t_1}{\partial \theta_1} & \cdots & \frac{\partial t_1}{\partial \theta_m} \\ \vdots & \ddots & \vdots \\ \frac{\partial t_k}{\partial \theta_1} & \cdots & \frac{\partial t_k}{\partial \theta_m} \end{pmatrix}. \quad (18)$$

If we define the extended model parameter vector as $\vec{\delta} = \left(\vec{x}, \vec{\theta}\right)$, then the full covariance matrix Σ between $\left(\vec{x}, \vec{\theta}\right)$ is expressed as:

$$\Sigma = \begin{pmatrix} M_x^{marg} & M_{x,\theta} \\ M_{x,\theta}^T & M_\theta \end{pmatrix}. \quad (19)$$

The cross-covariance term $M_{x,\theta}$ is calculated by introducing "variance penalty" terms [25]. The "variance penalty" is a measure of the contribution of the uncertainty of the nuisance variables to the variance of the calculated quantity $\vec{t}$. The cross-covariance term is:

$$M_{x,\theta} = -\left(G_x^T G_x\right)^{-1} G_x^T G_\theta M_\theta. \quad (20)$$

The following section explains how the generalized least-square method and the marginalization technique were applied to calculate the covariance matrix between the CAB model parameters.

5 Covariance matrix between the CAB model parameters

5.1 The CAB model parameter vector

The parameters of the CAB model were explained in Section 3.1 and are listed in Table 1. The parameter q_M (dummy atom charge) will be omitted in the analysis because it is redundant with the hydrogen charge q_H. The CAB model parameter vector $\vec{x}$ is:

$$\vec{x} = (\varepsilon_0, \sigma_0, q_H, D_{\mathrm{OH}}, \beta_{\mathrm{OH}}, d_{\mathrm{OH}}, k_\theta, \theta_{\mathrm{OH}}, d_{OM}). \quad (21)$$

The aim of the present work is not to produce a new set of best-estimate water potential parameters. That task was already accomplished in reference [10]. Therefore, as already indicated in Section 3.4, the objective is to generate variances and covariances between the CAB model parameters at 294 K without changing their values (retroactive approach) [26].

5.2 The nuisance parameter vector

For determining the covariances between the CAB model parameters, we have used the experimental average cosine of the scattering angle shown in Figure 2, and the total cross sections presented in Figure 3.

The experimental total cross sections were converted in transmission coefficient as follows:

$$T(E_n) = Ne^{-n\sigma_t(E_n)} + B, \quad (22)$$

where n is the sample areal density in atoms per barns, N represents the normalization and B stands for a "pseudo" background correction. Figure 4 compares the theoretical curves calculated with the CAB model at 294 K and the experimental transmission data reported by Heinloth [17], Herdade [18] and Dritsa [19]. The total cross section measured by Zaitsev et al. [16] was not converted to transmission because the sample thickness used in the experiment was not given by the author.

The reported cross section uncertainties account for the statistical and sample areal density uncertainties. The contribution of the latter ones was subtracted to be included in the marginalization procedure. The statistical uncertainties has been taken into account in the fitting procedure.

Regarding the experimental temperature of the water sample, no information is available. In the present work, we have used an uncertainty of ±5 K at 294 K.

In the CAB model, the weight of the translational vibration mode ω_t (Sect. 3.2) and the bound scattering cross section of ^{1}H (σ_b^H) were derive from experimental data. Thus, they cannot be included in the fitting procedure like the water potential parameters. A relative uncertainty on ω_t of ±10% is assumed because no information is published. Regarding the σ_b^H parameter, the relative uncertainty of ±0.2% recommended by the Neutron Standard Working Group of IAEA [27] was used:

$$\sigma_b^H = 20.478 \pm 0.041 b. \quad (23)$$

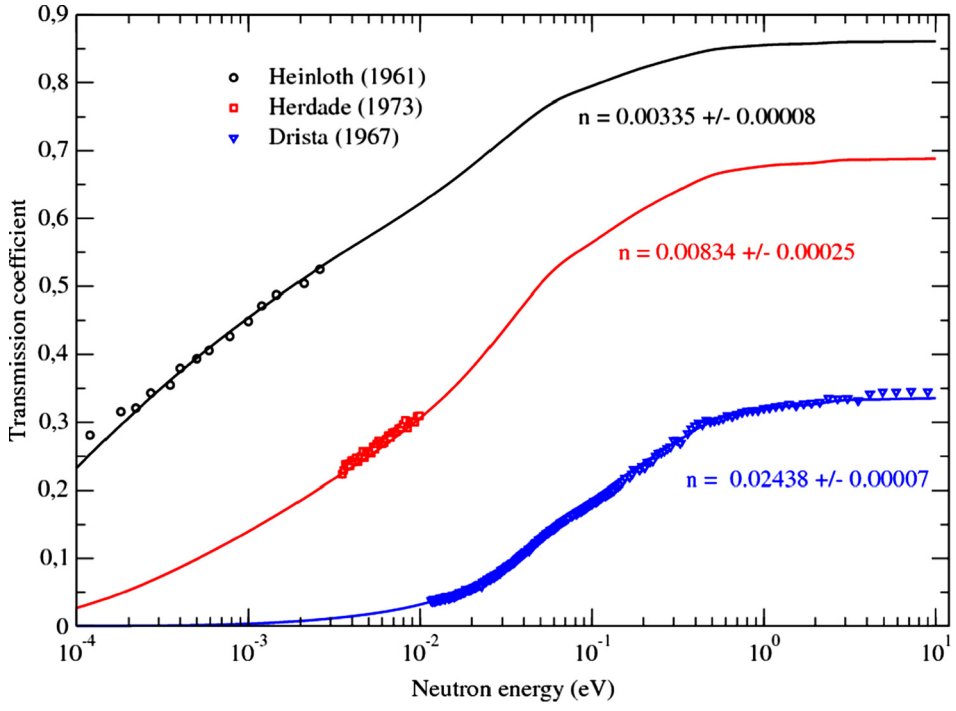

Fig. 4. Transmission coefficient at 294 K determined from the data reported in references [17–19].

Finally, the nuisance parameter vector is:

$$\vec{\theta} = \left(n, N, B, T, \omega_t, \sigma_b^H\right). \tag{24}$$

Table 3 summarizes the nuisance parameters with the uncertainties adopted for each experimental data set.

6 Results

The covariance matrix Σ between the model parameters was determined with the CONRAD code by using a two-step calculation scheme. The generalized least-square method provides the covariance matrix between the CAB model parameters M_x (Eq. (15)). Afterwards, these results are used in the marginalization technique to calculate the posterior covariance matrix M_x^{marg} (Eq. (17)).

At the beginning of the fitting procedure, it is assumed that the CAB model parameters are uncorrelated and have relative prior uncertainties of 1%. The posterior uncertainties reported in Table 4 are rather low. They lie below the prior uncertainties. The correlation matrix shows weak correlations between the parameters.

After the marginalization of the nuisance parameters, stronger correlations between the model parameters are calculated. Table 5 summarizes the relative uncertainties of the CAB model parameters and their correlations. Compared with the results after the fit, it can be seen that more realistic uncertainties are achieved.

The uncertainties range between 2 and 6%, excepted for the parameter ε_0, which is involved in the expression of the Lennard–Jones potential between the oxygens. Its relative uncertainty reaches 14.6%. Such result indicates that the calculated uncertainties on the CAB model parameters must be taken with care. If the parameters of the water potential remain within such 1σ uncertainties, then the forces between the atoms originated by the potentials would be severely modified. These perturbations would probably introduce unphysical changes at the level of the water molecule. Therefore, we have to keep in mind that the present results are only dedicated to generate usable uncertainties in applied neutronic field.

7 Uncertainties propagation of the CAB model parameters

7.1 Covariance matrix of the thermal scattering function

The thermal scattering function contains a very large number of values. To solve this difficulty, the $S(\alpha, \beta)$ values were averaged in 37 momentum transfer intervals. The average scattering function $\overline{S}_{ij}(\alpha_{ij}, \beta_0)$, for a given energy transfer β_0, is obtained as follows:

$$\overline{S}_{ij}(\alpha_{ij}, \beta_0) = \frac{\int_{\alpha_i}^{\alpha_j} (S\alpha, \beta_0) d\alpha}{\int_{\alpha_i}^{\alpha_j} d\alpha}. \tag{25}$$

Figure 5 shows the symmetric forms of $S(\alpha, \beta_0)$ and $\overline{S}(\alpha, \beta_0)$ as a function of the momentum transfer for $\beta_0 = 1.0$ calculated at 294 K. Figure 6 shows the relative uncertainties and the correlation matrix of the multigroup scattering function for two energy transfers ($\beta_0 = 1.0$ and 10.0). They were obtained from the propagation of the CAB model parameter uncertainties reported in Table 5.

Table 3. Uncertainties on the nuisance parameters (sample area density, normalization factor, background correction, temperature) for each experimental data introduced in the CONRAD calculations.

Parameter	Zaitsev et al. [16]	Heinloth [17]	Herdade [18]	Dritsa [19]	Beyster et al. [15]
$n(at)/b$	–	0.00335 ± 0.00008	0.00834 ± 0.00025	0.02438 ± 0.00007	–
N	1.0 ± 0.045	1.0 ± 0.01	1.0 ± 0.01	1.0 ± 0.01	1.0 ± 0.05
B	–	± 0.001	± 0.001	± 0.001	± 0.005
$T(K)$	294 ± 5	294 ± 5	294 ± 5	294 ± 5	294 ± 5

Table 4. Relative uncertainties and correlation matrix between the CAB model parameters after the fitting procedure.

Parameter	Value	Relative uncertainties	Correlation matrix								
σ_0 (kJ/mol)	0.31644	0.6%	100	−17	25	63	−31	−14	19	−25	19
ε_0 (nm)	0.7749	0.8%		100	−33	−3	−10	−16	1	−26	−15
q_H (e^-)	0.5564	0.7%			100	−51	−18	−13	12	−25	15
d_{OH} (nm)	0.09419	0.7%				100	5	−14	−16	−5	5
D_{OH} (kJ/mol)	432.581	0.8%					100	−31	15	−22	−2
β_{OH} (1/nm)	22.87	0.7%						100	−7	−24	4
θ_{OH} (°)	107.4	0.9%							100	−4	−9
k_θ (kJ/mol/rad^2)	367.81	0.8%								100	−10
d_{OM} (nm)	0.13288	0.7%									100

Table 5. Relative uncertainties and correlation matrix between the CAB model parameters after the marginalization.

Parameter	Value	Relative uncertainties	Correlation matrix								
σ_0 (nm)	0.31644	2.3%	100	−77	93	69	33	−18	−64	83	−14
ε_0 (kJ/mol)	0.7749	14.6%		100	−71	−98	−85	53	97	−54	−32
q_H (e^-)	0.5564	3.2%			100	59	28	−2	−60	81	−18
d_{OH} (nm)	0.09419	6.3%				100	89	−63	−96	44	38
D_{OH} (kJ/mol)	432.581	6.2%					100	−63	−88	6	57
β_{OH} (1/nm)	22.87	4.2%						100	51	−11	−28
θ_{OH} (°)	107.4	6.4%							100	−45	−9
k_θ (kJ/mol/rad^2)	367.81	3.8%								100	−14
d_{OM} (nm)	0.13288	2.7%									100

In both cases the relative uncertainties on the $\overline{S}_{ij}(\alpha_{ij}, \beta_0)$ function range between 10% in the peak of the distribution up to approximately 30% in the wings.

7.2 Covariance matrix of the ^{1}H in H_2O scattering cross section

The left-hand plot of Figure 7 shows the relative uncertainties and the correlation matrix of the ^{1}H in H_2O scattering cross section after the uncertainty propagation of the CAB model parameters at 294 K. Figure 8 compares the theoretical curve with the experimental data introduced in the CONRAD calculations.

Uncertainties and correlations reported in Table 5 provide realistic uncertainties on the scattering cross section. At the thermal neutron energy (25.3 meV), the relative uncertainty reaches approximately 3.3%. Beyond 1 eV, the uncertainty, mainly driven by the relative uncertainty of the bound scattering cross section of hydrogen, is close to 0.9%.

The spurious structures seen between 1 and 5 eV might be originated from the transition to the short collision time approximation used in LEAPR to calculate the TSL.

7.3 Covariance matrix of the average cosine $\overline{\mu}$ of the scattering angle

The right-hand plot of Figure 7 shows the relative uncertainties and the correlation matrix of the average cosine of the scattering angle at 294 K. At the thermal energy, the relative uncertainty is approximately 12%.

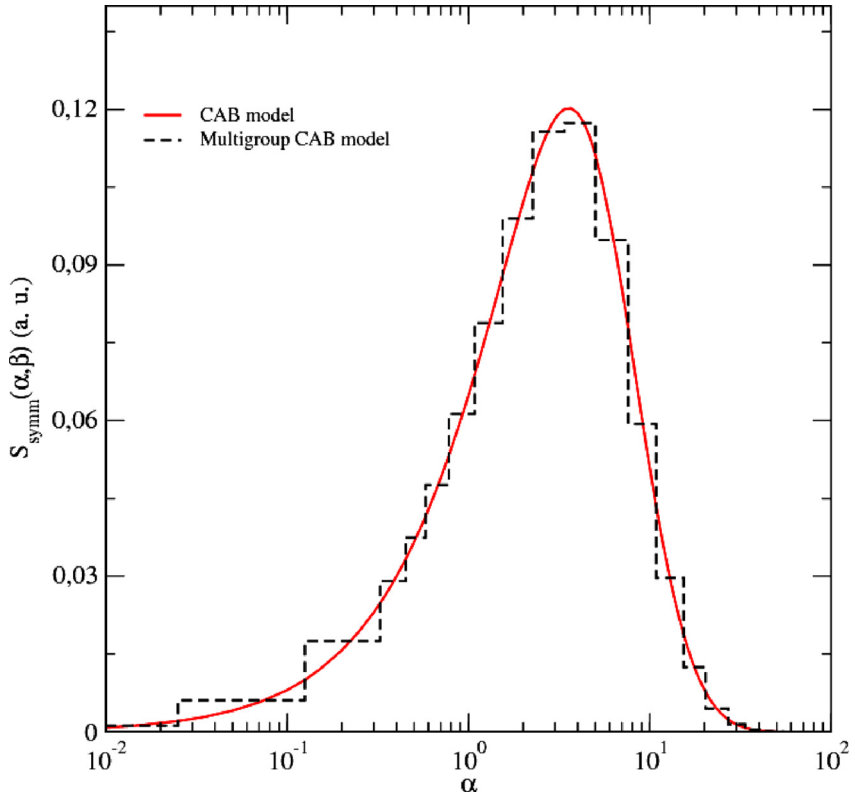

Fig. 5. Thermal scattering function $S(\alpha, \beta_0)$ and its multigroup representation $\overline{S}(\alpha, \beta_0)$ as a function of the momentum transfer for $\beta_0 = 1.0$ calculated with the CAB model at 294 K.

The bottom plot of Figure 8 compares the calculated $\overline{\mu}$ with the data used in the CONRAD analysis. The obtained uncertainties bands overlap the data over the full energy range.

7.4 Propagation to integral calculations

One of the main goals of the present work is to quantify the uncertainty due to the TSL of ^{1}H in H_2O in integral calculations. The performances of our covariance matrix between the CAB model parameters was investigated on the MISTRAL-1 and MISTRAL-2 configurations carried out in the EOLE critical facility of CEA Cadarache (France).

7.4.1 The MISTRAL experimental program

A detailed description of the experiments can be found in reference [28]. The reactivity excess was measured at "cold" reactor conditions, from 10 to 80 °C.

The MISTRAL-1 configuration is an UO_2 core (3.7% enriched in ^{235}U), while the MISTRAL-2 configuration is a MOX core (7.0% enriched in Am-PuO_2). Examples of radial cross section of the cores are shown in Figure 9. In the first case the criticality is reached by adjusting the boron concentration in the moderator. In the second case, the critical size of the core was adequately modified (8.7% fuel pins enriched in Am-PuO_2).

7.4.2 Propagation of the CAB model uncertainties to the MISTRAL calculations

The Monte-Carlo code TRIPOLI4® [29] was used to calculate the reactivity of MISTRAL-1 and -2, as a function of the temperature [30].

When the TSL of the CAB model is introduced in the JEFF-3.1.1 library [31], the differences $\Delta\rho$ between the calculated and experimental reactivities for MISTRAL-1 (UOX core) at 20 and 80 °C are close to 300 pcm:

$$\Delta\rho(20°C) = 283 \pm 71\,\text{pcm},$$

$$\Delta\rho(80°C) = 286 \pm 155\,\text{pcm}.$$

For MISTRAl-2 (MOX core), they reaches 900 pcm:

$$\Delta\rho(20°C) = 900 \pm 110\,\text{pcm},$$

$$\Delta\rho(80°C) = 869 \pm 203\,\text{pcm}.$$

The large discrepancies observed for the MOX core are due to the contribution of the ^{241}Am capture cross section, which is significantly underestimated in the JEFF-3.1.1 library.

The quoted uncertainties account for the statistical uncertainties due to the Monte-Carlo simulations (±25 pcm) and the uncertainty due to the TSL of ^{1}H in H_2O (Tab. 5). The later contribution was determined by a direct perturbation of the CAB model parameters.

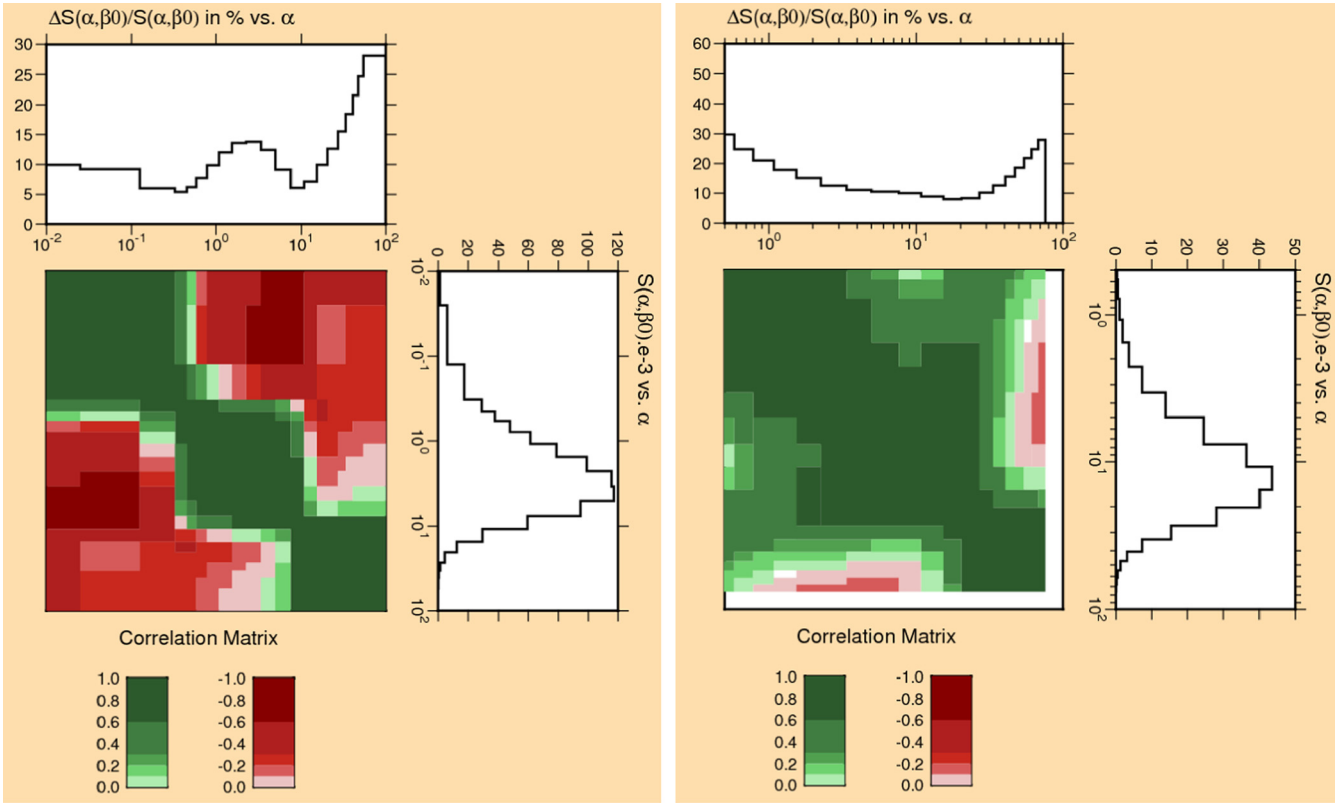

Fig. 6. Relative uncertainties and correlation matrix of the $\overline{S}(\alpha, \beta_0)$ functions for $\beta = 1.0$ (left-hand plot) and $\beta = 10.0$ (right-hand plot) calculated with the CAB model at 294 K with the uncertainties reported in Table 5.

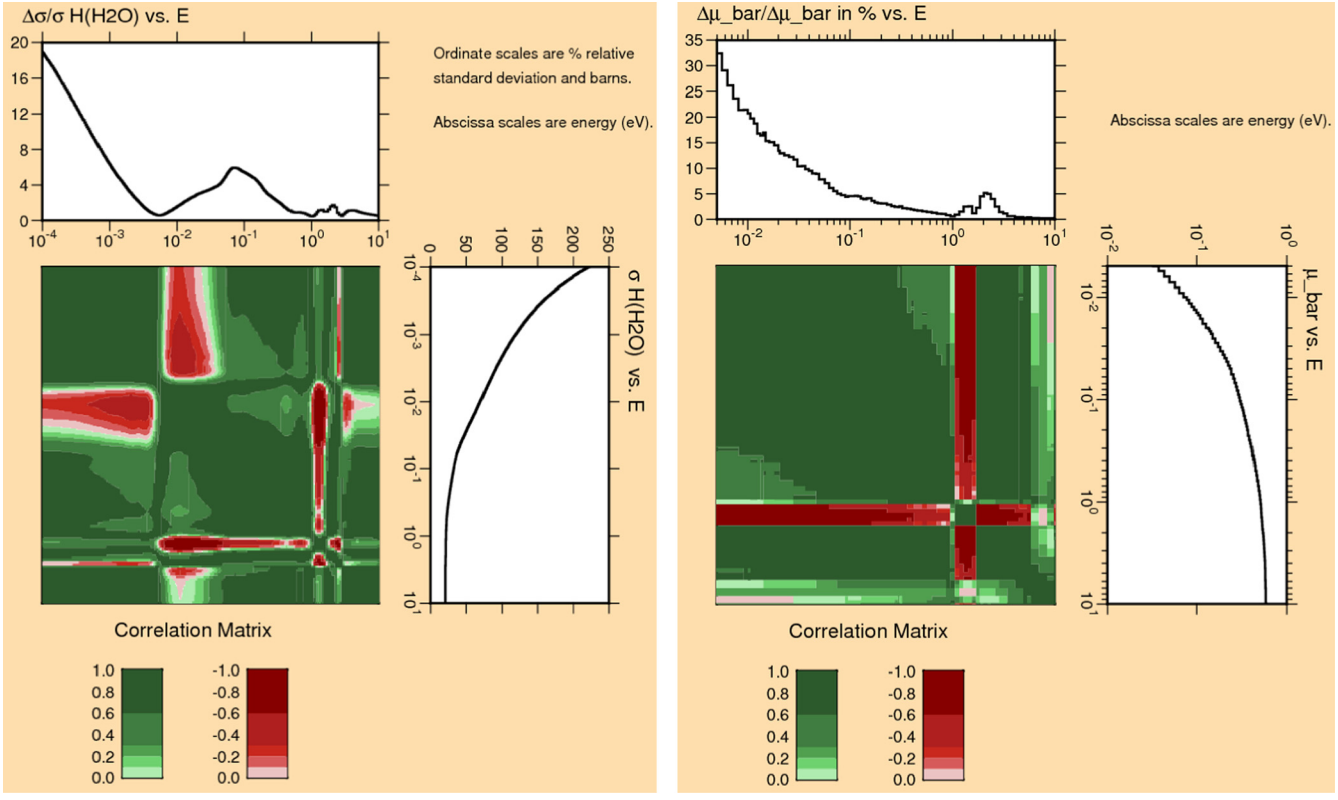

Fig. 7. Relative uncertainties and correlation matrix of the ^{1}H in H_2O scattering cross section (left-hand plot) and of the average cosine $\overline{\mu}$ of the scattering angle (right-hand plot) calculated with the CAB model at 294 K with the uncertainties reported in Table 5.

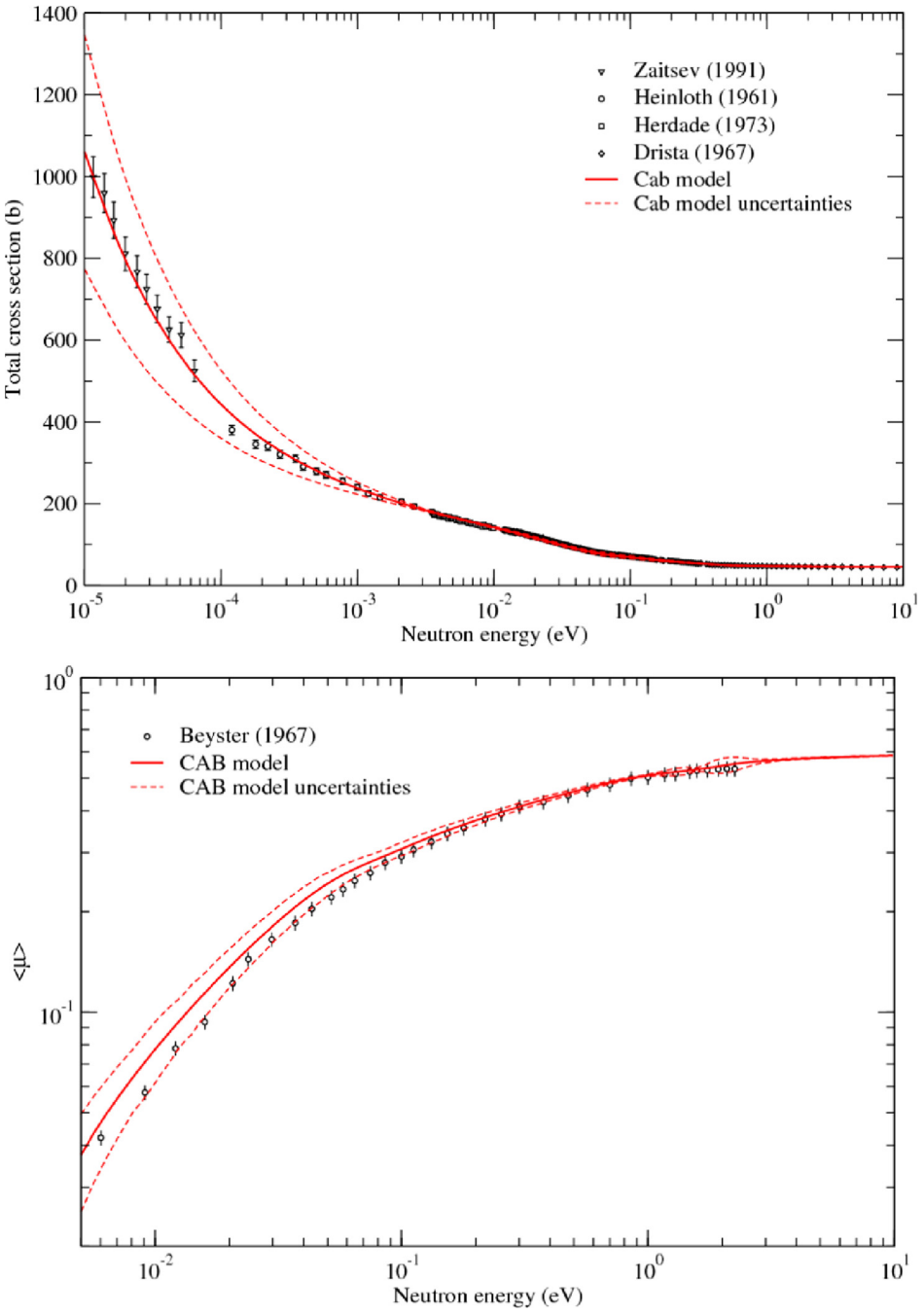

Fig. 8. Comparison of the theoretical scattering cross section (top plot) and of the average cosine $\overline{\mu}$ of the scattering angle (bottom plot) with the experimental data introduced in the CONRAD calculations.

At room temperature, the low uncertainty of 71 pcm indicates that the uncertainty on the TSL of light water coming from the CAB model could become a negligible contribution in many UOX configurations. This assumption is confirmed by the results reported in Table 6. For a standard UOX cell, it appears that the uncertainty on the capture cross section of hydrogen (±150 pcm) is even more important than the contribution due to the scattering process.

However, the present results confirms the higher sensitivity of the MOX cores to the TSL of light water. This trend is due to the large resonances in the cross sections of the Pu isotopes. In that case, the uncertainty of 110 pcm obtained at room temperature is no longer negligible. This is also confirmed in Table 7 by comparing the various contributions to the final uncertainty on the reactivity calculated for a MOX cell.

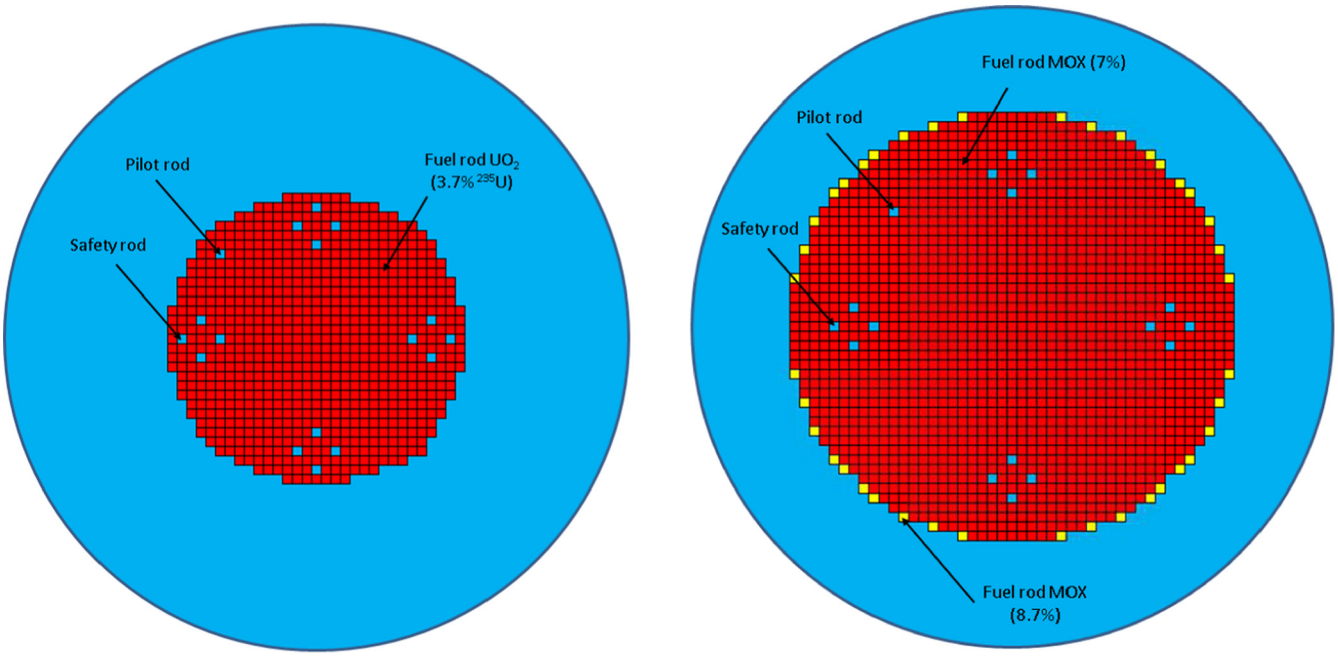

Fig. 9. Radial cross sections of the MISTRAL-1 core (left-hand plot) and the MISTRAL-2 core (right-hand plot) at $T = 20$°C.

Table 6. Example of uncertainties on the reactivity (UOX configuration at room temperature) in pcm due to the nuclear data. The contribution of ^{1}H in H_2O comes from the present work. The other contributions were calculated with the covariance data base COMAC [32] developed at the CEA of Cadarache.

Isotopes	(n,f)	Capture	(n,n)	(n,n′)	(n,xn)	ν_{tot}	χ_{fast}	χ_{th}	Total
^{1}H in H_2O		150	71						166
^{10}B		26							26
^{16}O		97	14	2					98
^{90}Zr		11	72	4					72
^{91}Zr		27	30	2					40
^{92}Zr		27	20	2					33
^{94}Zr		2	8	2					8
^{96}Zr		2	6						6
^{234}U	1	6	2						6
^{235}U	104	174	13			276		142	371
^{236}U		1							1
^{238}U	29	165	83	38	18	32	9		195
Total	108	303	137	39	18	277	9	142	470

8 Conclusions

The present work presents the methodology for generating the covariance matrix between the CAB model parameters, which describes the neutron scattering with the hydrogen bounded to the light water molecule. The covariance matrix has been calculated by using the generalized least-square and marginalization algorithms implemented in the CONRAD code.

The obtained uncertainties were propagated to produce covariance matrices for the thermal scattering function. A multigroup treatment on the momentum transfer was adopted to handle the large amount of data contained in the $S(\alpha, \beta)$ function.

Covariance matrices for the ^{1}H in H_2O scattering cross section and for the average cosine of the scattering angle were also produced. The calculated uncertainty bands in both cases overlap the experimental data selected for the

Table 7. Example of uncertainties on the reactivity (MOX configuration at room temperature) in pcm due to the nuclear data. The contribution of ^{1}H in H_2O comes from the present work. The other contributions were calculated with the covariance data base COMAC [32] developed at the CEA of Cadarache.

Isotopes	(n,f)	Capture	(n,n)	(n,n′)	(n,xn)	ν_{tot}	χ_{fast}	χ_{th}	Total
^{1}H in H_2O		46	110						119
^{10}B		8							8
^{16}O		114	24	4					117
^{90}Zr		11	24	7					27
^{91}Zr		13	16	4					21
^{92}Zr		8	22	4					24
^{94}Zr		2	59	3					59
^{96}Zr		2	13	1					14
^{235}U	2	6	3	1		5		4	9
^{238}U	114	88	80	−60	25	35	12		160
^{238}Pu	1	70	−20	1		9	1		67
^{239}Pu	278	371	26	5		57	0	126	484
^{240}Pu	42	178	−16	−5	1	2	9		182
^{241}Pu	108	96	8			88	58		179
^{242}Pu	3	131	10	2		2	1		131
^{241}Am	−3	47	2	29		1			47
Total	322	475	156	−59	25	111	60	126	619

CONRAD analysis. The present methodology allows obtaining realistic uncertainties on the cross section. At the neutron thermal energy, the relative uncertainty is 3.3%.

The contribution of the uncertainty due to the ^{1}H in H_2O thermal scattering data was then evaluated on the MISTRAL-1 (UOX) and MISTRAL-2 (MOX) integral experiments carried out in the EOLE facility of CEA Cadarache. The calculated uncertainty at 20 °C reaches ±71 pcm for the MISTRAL-1 core. At 80 °C, the uncertainty is almost twice with respect to room temperature. The same trend was found for the MISTRAL-2 configuration, where the uncertainty on the reactivity is ±110 pcm at 20 °C. The present results highlight the quality of the CAB model for calculating the TSL of light water at room temperature. For UOX configurations, we can expect a negligible contribution on the final uncertainty in nuclear criticality and safety studies.

The authors would like to thank P. Tamagno and P. Archier, from CEA Cadarache, for sharing their calculations on the reactivity breakdown for the UOX and MOX configurations.

Author contribution statement

Parameters of the Molecular Dynamic simulation were established by J.I Marquez Damian with the GROMACS code. The determination of the covariance matrix between the GROMACS parameters and the propagation of the uncertainties were performed by J.P. Scotta and G. Noguere by using the CONRAD code.

References

1. J.C. Holmes, A.I. Hawari, M. L. Zerkle, Nucl. Sci. Eng. **184**, 84 (2016)
2. G. Noguere, J.P. Scotta, C. de Saint Jean, P. Archier, Ann. Nucl. Energy **104**, 132 (2017)
3. M. Mattes, J. Keinert, Thermal Neutron Scattering Data for the moderator Materials H_2O, D_2O and ZrH_x in ENDF-6 Format and as ACE Library for MCNP(X) Codes, International Atomic Energy Agency Report INDC(NDS) 0470, 2005
4. J.I. Marquez Damian, J.R. Granada, D.C. Malaspina, Ann. Nucl. Energy **65**, 280 (2014)
5. G.L. Squires, *Introduction to the Theory of Thermal Neutron Scattering* (Cambridge University Press, New York, 1977)
6. R.E. MacFarlane, New Thermal Scattering Files for ENDF/B-VI Release-2, Los Alamos National Laboratory Report LA-12639-MS, 1994
7. L. Van Hove, Phys. Rev. **95**, 249 (1954)
8. D.W. Muir, R.M. Boicourt, A.C. Kahler, The NJOY Data Processing System, Version 2012, Los Alamos National Laboratory Report LA-UR-12-27079, 2012
9. D. Van Der Spoel et al., J. Comput. Chem. **26**, 1701 (2005)
10. M.A. Gonzalez, J.L.F. Abascal, J. Chem. Phys. **135**, 224516 (2011)
11. P.A. Egelstaff, P. Schofield, Nucl. Sci. Eng. **12**, 260 (1962)
12. V. Jaiswal et al., EPJ Web Conf. **146**, 13006 (2017)
13. F. Real et al., J. Chem. Phys. **139**, 114502 (2013)
14. A.G. Novikov et al., J. Struct. Chem. **31**, 77 (1990)
15. J.R. Beyster, J.C. Young, J.M. Neill, W.R. Mowry, Differential Neutron Scattering from Hydrogenous Materials, General Atomics Technical Report GA- 6295, 1965
16. K.N. Zaitsev et al., Sov. At. Energy **70**, 238 (1991)
17. K. Heinloth, Z. Phys. **163**, 218 (1961)

18. S.B. Herdade, Progress Report on Nuclear Data in Brazil (June 1971–May 1972), International Atomic Energy Agency Report INDC(BZL)-4, 1973
19. M. Dritsa, A. Kostikas, Total Cross Section of Water at Room Temperature and 200 °C, OECD Nuclear Energy Agency Report EANDC(OR)-63L, 1967
20. P. Archier et al., Nucl. Data Sheets **118**, 488 (2014)
21. T. Bayes, An essay toward solving a problem in the doctrine of chances, Philos. Trans. R. Soc. London **53**, 370 (1763) [reprinted in Biometrik **45**, 293 (1958)]
22. D. Smith, in *Probability, Statistics and Data Uncertainties in Nuclear Science and Technology* (OECD Nuclear Energy Agency Committee Series, 1990), Vol. 4
23. C. de Saint Jean et al., Nucl. Sci. Eng. **161**, 363 (2009)
24. G. Noguere, P. Archier, C. de Saint Jean, B. Habert, Nucl. Sci. Eng. **172**, 164 (2012)
25. D.W. Muir, Nucl. Instrum. Methods A **644**, 55 (2011)
26. B. Habert et al., Nucl. Sci. Eng. **166**, 276 (2010)
27. A.D. Carlson et al., Nucl. Data Sheets **110**, 3215 (2009)
28. S. Cathalau et al., MISTRAL: an experimental program in the EOLE facility devoted to 100% MOX core physics, in *Proceeding of International Conference on Physics of Reactors, PHYSOR 1996*, *Mito, Japan, 1996*
29. E. Brun et al., Ann. Nucl. Energy **82**, 151 (2015)
30. J.P. Scotta, G. Noguere, D. Bernard, J.I. Marquez Damian, A. Santamarina, EPJ Nucl. Sci. Technol. **2**, 28 (2016)
31. A. Santamarina et al., The JEFF-3.1.1 Nuclear Data Library, JEFF Report 22, Nuclear Energy Agency, 2009
32. P. Archier et al., COMAC: nuclear data covariance matrices library for reactor applications, in *Proceeding of International Conference on Physics of Reactors, PHYSOR 2014, Kyoto, Japan, 2014*

Cite this article as: Juan Pablo Scotta, Gilles Noguère, Jose Ignacio Marquez Damian, Generation of the ^{1}H in H_2O neutron thermal scattering law covariance matrix of the CAB model, EPJ Nuclear Sci. Technol. **4**, 32 (2018)